relative to the crater diameter is very typical. Melt production increases with impact energy, such that only large craters are expected to produce significant quantities of melt (*31*). This melt is deposited as thin veneers, flows, and ponds (*32*), so that melt sufficient to affect the spectral reflectivity is expected to remain near the surface only for relatively large and young craters, postdating widespread resurfacing from impact basins. Smrekar and Pieters (*33*) showed that reflectance spectra of the anomalously red crater rings of Tycho and Copernicus are consistent with the presence of iron-bearing glass. The melt is concentrated near the crater rim because it is produced from the deepest ejected target material. Therefore, we expect that all craters larger than about 25 km in diameter and postdating the formation of the Imbrium basin will have anomalously red near-rim colors. This generalization is observed in the EM-2 data for the near-side craters Copernicus, Zucchius, Pythagoras, Carpenter, Philolaus, Plato, Archimedes, Theophilus, Langrenus, Plinius, Geminus, Fabricus, and Hainzel, as well as for the far-side craters Ohm, Vavilov, and Hausen (*5*). In the case of Copernican age craters, the spectral effects of fresh soils partly counteract the reddish melt, but they are still redder (and darker) than melt-free soils of similar age and composition. The most recent of the large Copernican age craters, such as Tycho, Jackson, and Kepler, have relatively red and dark rings as compared to crater interiors and outer ejecta and rays.

The flybys of the moon by Galileo in 1990 and 1992 provided calibrated multispectral coverage of about 75% of the lunar surface in the 400- to 1000-nm spectral region. The images cover well-characterized regions of the near side, including standard areas for remote sensing and sample sites, that have enabled the calibration of Galileo data for extrapolation to areas on the northern, eastern, and western limbs and the far side that previously lacked quantitative multispectral coverage.

REFERENCES AND NOTES

1. M. J. S. Belton *et al.*, *Science* **255**, 570 (1992).
2. J. W. Head *et al.*, *J. Geophys. Res.* **98**, 17149 (1993).
3. C. M. Pieters *et al.*, *ibid.*, p. 17127.
4. R. Greeley *et al.*, *ibid.*, p. 17183.
5. A. S. McEwen *et al.*, *ibid.*, p. 17207.
6. T. B. McCord, M. P. Charette, T. V. Johnson, L. A. Lebofsky, C. M. Pieters, *ibid.* **77**, 1349 (1972).
7. C. Pieters, *Proc. Lunar Planet. Sci. Conf.* **9**, 2825 (1978).
8. The SSI filter set is described by M. J. S. Belton *et al.* [*Space Sci. Rev.* **60**, 413 (1992)] and its relation to lunar compositional studies is described in (*1*).
9. B. K. Lucchitta, *U.S. Geol. Surv. Misc. Invest. Ser. Map I-1062* (1978).
10. D. E. Wilhelms, *U.S. Geol. Surv. Prof. Paper 1348* (1987), p. 1.
11. W. K. Hartmann and G. P. Kuiper, *Lunar Planet. Lab. Comm.* **1** (no. 12), plate 12.51 (1962).
12. T. V. Johnson *et al.*, *Proc. Lunar Planet. Sci. Conf.* **8**, 1013 (1977).
13. K. A. Howard, D. E. Wilhelms, D. H. Scott, *Rev. Geophys. Space Phys.* **12**, 309 (1974).
14. D. E. Wilhelms and J. F. McCauley, *U.S. Geol. Surv. Misc. Invest. Ser. Map I-703* (1971); N. J. Trask and J. F. McCauley, *Earth Planet. Sci. Lett.* **14**, 201 (1972); W. R. Muehlberger *et al.*, in "Apollo 16 Preliminary Science Report," *NASA SP-315* (1972), p. 6-1; G. E. Ulrich *et al.*, *U.S. Geol. Surv. Prof. Paper 1048* (1981), p. 1; J. M. Boyce *et al.*, *Proc. Lunar Planet. Sci. Conf.* **5**, 11 (1974); V. R. Oberbeck *et al.*, *Moon* **12**, 19 (1975).
15. G. Neukum, *Moon* **17**, 383 (1977); Habilitationsschriff, Ludwig Maximilianis Universität, Münich (1983); G. Neukum *et al.*, *Moon* **12**, 201 (1975).
16. P. H. Schultz and P. D. Spudis, *Proc. Lunar Planet. Sci. Conf.* **10**, 2899 (1979).
17. J. W. Head and L. Wilson, *Geochim. Cosmochim. Acta* **56**, 2155 (1992).
18. B. R. Hawke and J. F. Bell, *Proc. Lunar Planet. Sci. Conf.* **12**, 665 (1981); J. F. Bell and B. R. Hawke, *J. Geophys. Res.* **89**, 6899 (1984).
19. B. R. Hawke *et al.*, *Lunar Planet. Inst. Tech. Report 92-09* (1992), p. 14.
20. J. W. Head *et al.*, *Lunar Planet. Sci. Conf.* **24**, 629 (1993).
21. D. A. Williams, thesis, Arizona State University (1992); S. D. Kadel, thesis, Arizona State University (1993).
22. M. P. Charette, T. B. McCord, C. M. Pieters, J. B. Adams, *J. Geophys. Res.* **79**, 1605 (1974); M. P. Charette, L. A. Sodenblom, J. B. Adams, M. J. Gaffey, T. B. McCord, *Proc. Lunar Planet. Sci. Conf.* **7**, 2579 (1976).
23. M. R. Robinson, B. R. Hawke, P. G. Lucey, G. A. Smith, *J. Geophys. Res.* **97**, 18 (1992).
24. D. E. Wilhelms and F. El Baz, *U.S. Geol. Surv. Misc. Invest. Ser. Map I-948* (1977).
25. J. W. Head *et al.*, in *Mare Crisium: A View from Luna 24*, R. B. Merrill and J. J. Papike, Eds. (Pergamon, New York, 1978), pp. 43–74.
26. B. L. Barsukov *et al.*, *Proc. Lunar Planet. Sci. Conf.* **8**, 3319 (1977).
27. L. R. Gaddis, C. M. Pieters, B. R. Hawke, *Icarus* **61**, 461 (1985).
28. L. Wilson and J. Head, *J. Geophys. Res.* **86**, 2971 (1981).
29. G. Heiken *et al.*, *Geochim. Cosmochim. Acta* **38**, 1703 (1974).
30. B. R. Hawke *et al.*, *Proc. Lunar Planet. Sci. Conf.* **21**, 377 (1991).
31. R. A. F. Grieve *et al.*, in *Impact and Explosion Cratering*, D. J. Roddy, R. O. Pepin, R. B. Merrill, Eds. (Pergamon, New York, 1977), pp. 791–814.
32. B. R. Hawke and J. W. Head, *ibid.*, p. 815.
33. S. Smrekar and C. M. Pieters, *Icarus* **63**, 442 (1985).

34. We thank the Galileo Project Office, the National Aeronautics and Space Administration (NASA), and numerous individuals who participated in the mission planning and initial data analysis, including C. Avis, T. Becker, L. Bolef, N. Bridges, C. Cunningham, E. DeJong, K. Edwards, E. Fischer, R. Garstang, A. Harch, S. Kadel, R. Kirk, J. Moersch, J. Plutchak, M. Robinson, R. Sullivan, W. Sullivan, J. Sunshine, S. Vail, L. Wainio, D. Williams, and J. Yoshimizu. The Galileo data set is available on CD-ROM through the NASA Planetary Data System. The National Optical Astronomy Observatories are operated by AURA, Inc., under a cooperative agreement with the National Science Foundation.

17 September 1993; accepted 24 March 1994

Rechargeable Lithium Batteries with Aqueous Electrolytes

Wu Li, J. R. Dahn,* D. S. Wainwright

Rechargeable lithium-ion batteries that use an aqueous electrolyte have been developed. Cells with $LiMn_2O_4$ and VO_2(B) as electrodes and 5 M $LiNO_3$ in water as the electrolyte provide a fundamentally safe and cost-effective technology that can compete with nickel-cadmium and lead-acid batteries on the basis of stored energy per unit of weight.

During the 1970s and 1980s, rechargeable lithium batteries were touted by some researchers as providing a possible long-term solution to the electric vehicle (EV) battery problem. The cells had about twice the energy density (measured by watt-hours stored per kilogram of battery) of the best competing ambient temperature batteries. Many companies moved to commercialize the technology, beginning with small cells for consumer applications, in view of the large markets anticipated. These cells used lithium metal as the negative electrode, a transition metal oxide [such as MnO_2 (*1*)] or chalcogenide [such as $NbSe_3$ (*2*)] as the positive electrode, and a nonaqueous electrolyte containing dissolved Li ions.

The operation of such cells is based on the ability of the positive electrode material to reversibly "intercalate" Li. Intercalation is the insertion of a guest atom (Li, for instance) into a host solid (such as MnO_2), accompanied by only slight, reversible structural changes in the host. Hosts for intercalation are commonly layered compounds such as graphite (*3*) or tunnel compounds such as MnO_2 or $LiMn_2O_4$ (*4*), in which the intercalated Li can reside between the layers or in the tunnels. Intercalation of Li occurs because the chemical potential of Li can be lowered when the Li atom is inserted into the host, thus forming chemical bonds.

The binding energy of Li when intercalated into a variety of hosts has been measured with respect to the binding energy of Li metal (Fig. 1). In each of the hosts listed,

W. Li and J. R. Dahn, Department of Physics, Simon Fraser University, Burnaby, British Columbia, Canada V5A 1S6.

D. S. Wainwright, Moli Energy (1990) Limited, 20000 Stewart Crescent, Maple Ridge, British Columbia, Canada V2X 9E7.

*To whom correspondence should be addressed.

the Li atoms can diffuse readily within the host, even when the binding energy is near 4 eV. (LiF is included in the figure for reference, but it is not an intercalation compound.) Because Li can be added to and removed from these materials, it is common to designate them as Li_x(Host), with x designating the Li stoichiometry.

The voltage and operation of cells with negative electrodes of Li metal are now easy to understand. During the discharge of the cell, Li at the negative electrode dissociates into ions and electrons that move to the positive electrode through the electrolyte and the external circuit, respectively. The ions and electrons meet at the surface of the positive electrode, where they intercalate within the host material. The open circuit voltage of the cell is given by the binding energy of Li in the host (in electron volts), divided by the electron charge. (Formally, the cell voltage is given by the difference between the chemical potential of Li in the intercalation host and in Li metal, divided by the charge on the electron.) To recharge the cell, a charger is used to extract electrons and the corresponding ions from the host, and Li metal is replated on the negative electrode.

Rechargeable cells with negative electrodes of Li metal can be made that have excellent performance characteristics (*1*, *2*). However, it seems difficult to make them safe (*5*). At the heart of the safety problem is the reactivity of metallic Li with the nonaqueous electrolytes used in these cells. Lithium reacts instantly with these electrolytes to form a passivating film of insoluble reaction products on the Li metal surface. Once the film is about 50 Å thick, the reaction stops. Although the film is a Li-ion conductor, it is an electronic insulator that prevents the transport of Li atoms to the electrolyte, once the film thickness is greater than the electron tunneling length. However, as cells are repeatedly charged and discharged, the Li metal becomes very porous, and the area of contact between Li and electrolyte becomes very large. After several hundred cycles, such cells become prone to safety problems (such as producing intense smoke or even fire) if they reach temperatures above about 120°C because of mechanical or electrical abuse. This problem led to a major product recall in 1989 involving cells manufactured by Moli Energy (Burnaby, British Columbia, Canada) (*5*). Most other Li battery introductions planned by other firms were then abandoned.

To solve the safety problem associated with Li metal, battery scientists eliminated Li metal but tried to retain the high energy density attainable with the technology. The so-called Li-ion cells use two different intercalation hosts as the positive and negative electrodes. For example, Sony Energytec introduced the 3.5-V $LiCoO_2$/carbon cell in 1992, and it has been very successful (*6*). The Sony cell and others like it are currently the state-of-the-art power sources for consumer electronics. In such a cell, the electrode materials are chosen so that the chemical potential of Li in each differs by several electron volts, with the result that high energy density can still be maintained. Safety is also improved, because the surface area of the electrodes remains constant during cycling, even though Li-intercalated carbon is almost as reactive as metallic Li (see Fig. 1). It is unclear, however, whether cells large enough for EVs will be safe.

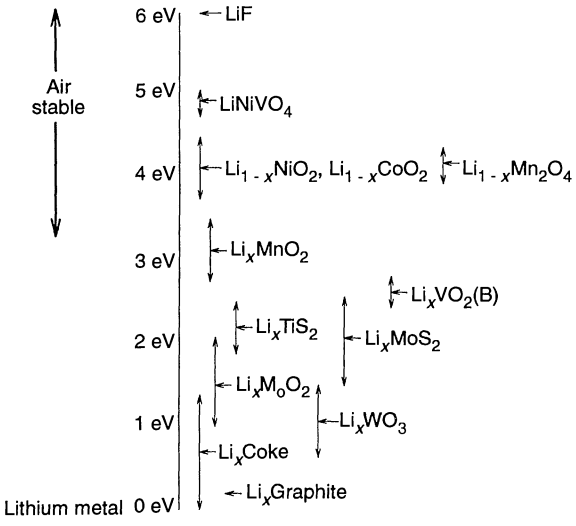

Fig. 1. The binding energy of Li, intercalated within a variety of materials, measured relative to that of Li metal.

The Li-ion technology is also expensive. Nonaqueous electrolytes have ion conductivities about two orders of magnitude lower than their aqueous counterparts, so cell designs incorporating thin electrodes (0.1 mm) must be used. Suitable Li salts, such as $LiPF_6$, are also expensive, as are the microporous films used to separate the electrodes and hold the electrolyte. Water must be rigorously excluded during some manufacturing steps, which leads to additional costs.

Lithium batteries were historically designed with metallic Li as one component, which precluded the consideration of water as an electrolyte solvent. The reaction product of Li and water, LiOH, is soluble in water, so that a passivating film does not form and a violent reaction occurs. Similarly, in the current generation of Li-ion cells that use Li-intercalated carbon as the negative electrode, water cannot be used as the electrolyte. However, once the Li in an intercalation host is sufficiently tightly bound (at about 3.2 ± 0.2 eV), it will not react with water to form LiOH and H_2 (*7*).

When a Li intercalation compound is put in water, one must consider whether the reaction

$$Li_x(\text{Host}) + xH_2O \Leftrightarrow \text{Host} + xLiOH(aq) + x/2H_2(g) \quad (1)$$

will occur. We recently showed (*8*) that intercalation compounds that are unstable in pure water can be made stable in concentrated LiOH solution. The chemical potential of Li^+ in solution increases with

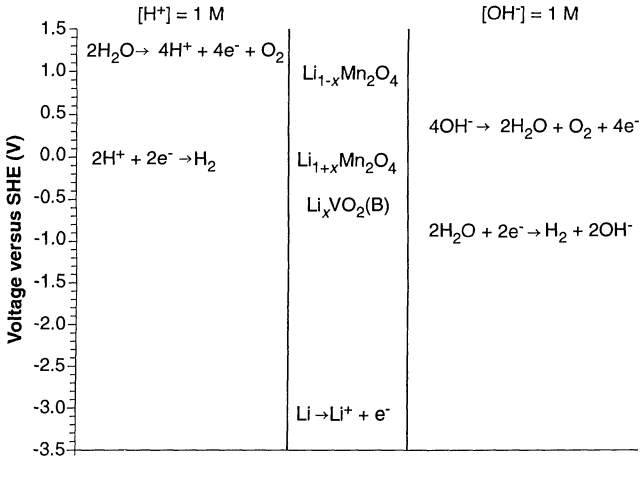

Fig. 2. The potentials of the indicated reactions versus the standard hydrogen electrode (SHE) in solutions where [Li^+] = 1.0 M. Both acidic and basic electrolytes with 1 M H^+ or 1 M OH^-, respectively, are considered.

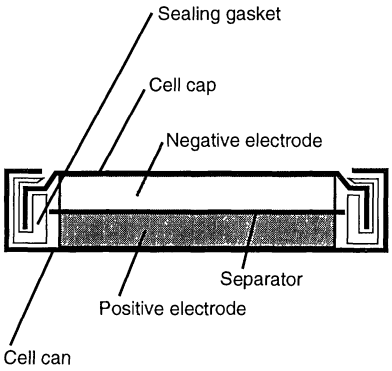

Fig. 3. A schematic of the coin cell used to test the aqueous Li-ion chemistry.

concentration and tends to drive Eq. 1 to the left. This suggests that Li-ion cells with aqueous electrolytes can be considered for appropriately chosen hosts.

We must also consider the potentials for oxygen and hydrogen evolution that can occur in aqueous electrolytes (Fig. 2). Figure 2 also shows the standard electrode potential for the reaction

$$Li \Leftrightarrow Li^+ + e^- \quad (2)$$

Figure 1 lists the chemical potentials of Li intercalation compounds relative to reaction 2, so we can locate electrode materials on Fig. 2, as we have done for the reactions

$$LiMn_2O_4 \Leftrightarrow Li_{1-x}Mn_2O_4 + xLi^+ + xe^- \quad (3)$$

and

$$VO_2(B) + xLi^+ + xe^- \Leftrightarrow Li_xVO_2(B) \quad (4)$$

["B" designates a particular crystal form of VO_2 (9).] In an appropriately chosen electrolyte, reactions 3 and 4 should be viable without excessive simultaneous production of O_2 or H_2. A cell based on reactions 3 and 4 will have a terminal voltage near 1.5 V.

We synthesized $LiMn_2O_4$ according to the methods described in (*10*) and $VO_2(B)$ according to the methods described in (*11*). Both of these materials are framework-type intercalation compounds. Tablet electrodes 8 mm in diameter and with a total mass of 0.10 g were prepared from each material. Carbon black (10% by weight) and ethylene propylene diene monomer binder (3% by weight) were added to the tablet mix to provide good electrical conductivity and good mechanical toughness. The mix was then pressed in 0.10-g allotments in a cylindrical die to the desired thickness (1.0 mm).

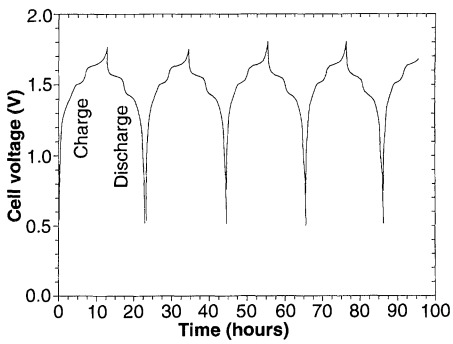

Fig. 4. The voltage plotted versus time as a $LiMn_2O_4/VO_2(B)$ cell is repeatedly charged and discharged. The currents used were ±1 mA. The cell test was carried out at 30°C.

Coin-type test cells were made with 1225 hardware (the first two numbers give the cell diameter in millimeters and the second two give the cell height in tenths of millimeters; a 1225 cell is 12 mm in diameter and 2.5 mm thick). First, the electrodes were thoroughly wetted with an aqueous solution that was 5.0 M in $LiNO_3$ and about 0.001 M in LiOH. A microporous polypropylene separator (Celgard 3500), which incorporates a wetting agent, was used to separate the electrodes as they were tightly crimped in the cell case. Figure 3 shows a schematic of the finished cell. Because the concentration of OH is 0.001 M in this cell, we expect the potentials for H_2 and O_2 evolution to shift up by about 0.175 V, compared with their positions in 1 M OH^-, as shown on the right of Fig. 2.

The cell was then charged with a current of 1 mA. During the charge, Li was extracted from $LiMn_2O_4$, producing $Li_{1-x}Mn_2O_4$, and intercalated into $VO_2(B)$, producing $Li_xVO_2(B)$. Figure 4 shows the voltage profile during this charging and during the next few charge-discharge cycles. The cell shows excellent reversibility, an average voltage near 1.5 V, and a capacity of 10 mA·hour.

We calculated the energy density of the cell using the weight of the electrodes, the cell voltage, and the cell capacity (we did not include the electrolyte or cell-case weight). This cell's energy density is 75 watt·hours/kg. Typically, the active electrode weights are about 50% of the total weight of practical cells, if the Sony Li-ion product is used as an example. Thus, practical energy densities near 40 watt·hours/kg can be expected for this chemistry when used in larger cells. Furthermore, the theoretical energy density for this cell is 112 watt·hours/kg, assuming 0.5 Li per transition metal can be cycled in each electrode and that the average cell voltage is 1.5 V. These assumptions would give about 55 watt·hours/kg in a practical cell, which is competitive with both Pb-acid (about 30 watt·hours/kg) and Ni-Cd (about 50 watt·hours/kg) technologies.

In basic electrolytes, O_2 evolution at $Li_{1-x}Mn_2O_4$ may occur simultaneously with the removal of Li from the electrode, as indicated in Fig. 2. (This is analogous to the O_2 evolution that occurs in Ni-Cd cells during charging.) The O_2 should then diffuse to the $Li_xVO_2(B)$ electrode, where it will recombine with water and electrons to produce OH^- again. Therefore, it should be possible to select electrolytes of appropriate pH that allow for efficient charging of the positive electrode and that also provide effective oxygen pressure control.

The $LiMn_2O_4/VO_2(B)$ couple by no means represents the optimum electrode pair for the aqueous Li-ion cell. Many types of Li manganese oxides are known to intercalate Li in the right chemical potential range for this type of cell (*12*). One approach to an extremely low-cost system would be to use $LiMn_2O_4$ for both electrodes. Because Li can be extracted from $LiMn_2O_4$ (to form $Li_{1-x}Mn_2O_4$) at 4 V versus Li and added to $LiMn_2O_4$ (to form $Li_{1+x}Mn_2O_4$) at about 3 V versus Li, a 1-V cell would result. Manganese and its oxides are cheap, plentiful, and less toxic than Ni and Co oxides, so a $Li_{1+x}Mn_2O_4/Li_{1-x}Mn_2O_4$ cell could have an enormous potential market.

In a 1989 review of about 40 battery technologies for EV applications, Ratner *et al.* (*13*) concluded that there was no suitable technology currently available for electric vehicles. The review considered factors such as cost, safety, performance, and environmental friendliness. Today, the search for an acceptable EV battery continues. For example, the Ni-metal hydride battery developed by Ovonics (Warren, Michigan) has been shown to attain 80 watt·hours/kg in sizes acceptable for EVs (*14*). However, some industry experts contend that the Ni-metal hydride technology is too expensive and is not environmentally acceptable for EV applications. It is our opinion that the aqueous Li-ion approach described here shows promise and needs to be included in the hunt for the EV battery.

REFERENCES AND NOTES

1. K. Brandt, paper presented at the Fourth International Seminar on Lithium Battery Technology and Applications, Deerfield Beach, FL, 5 to 7 March 1989.
2. J. Broadhead, in *Proceedings of the Third Annual Battery Conference on Applications and Advances*, California State University, Long Beach, CA, 12 to 18 January 1988; S. Basu and F. A. Trumbore, *J. Electrochem. Soc.* **139**, 3379 (1992).
3. M. S. Dresselhaus and M. Endo, in *Graphite Intercalation Compounds II*, H. Zabel and S. A. Solin, Eds. (Springer-Verlag, Berlin, 1992), pp. 347–407; J. R. Dahn *et al.*, *Electrochim. Acta* **38**, 1179 (1993).
4. M. M. Thackeray *et al.*, *J. Electrochem. Soc.* **139**, 363 (1992); M. M. Thackeray and R. J. Gummow, U.S. Patent 5,240,794 (1993).
5. For example, see "Cellular phone recall may cause setback for Moli," *Toronto Globe and Mail (Canada)*, 15 August 1989.
6. T. Nagaura and K. Tozawa, *Prog. Batteries Solar Cells* **9**, 209 (1990); G. Stix, *Sci. Am.* **269**, 108 (October 1993).
7. J. R. Dahn, U. von Sacken, M. W. Juzkow, H. Al-Janaby, *J. Electrochem. Soc.* **138**, 2207 (1991).
8. W. Li, W. R. McKinnon, J. R. Dahn, *ibid.*, in press.

9. W. Theobald *et al.*, *J. Solid State Chem.* **17**, 431 (1976); D. W. Murphy *et al.*, *J. Electrochem. Soc.* **128**, 2053 (1981).
10. T. Ohzuku, M. Kitagawa, T. Hirai, *J. Electrochem. Soc.* **137**, 769 (1990).
11. J. R. Dahn, T. van Buuren, U. von Sacken, U.S. Patent 4,965,150 (1990).
12. For example, see T. Ohzuku, A. Ueda, T. Hirai, *Chem. Express* **7**, 193 (1992); T. Nohma, T. Saito, N. Furukawa, H. Ikeda, *J. Power Sources* **26**, 389 (1989); J. M. Tarascon and D. Guyomard, *Electrochim. Acta* **38**, 1221 (1993).
13. E. Z. Ratner, P. C. Symons, W. Walsh, C. J. Warde, G. L. Hendriksen, "Assessment of battery technologies for electric vehicles," contract DE-AC07-76IDO1570 (U.S. Dept. of Energy, Washington, DC, August 1989).
14. S. R. Ovshinsky, M. A. Fetcenko, J. Ross, *Science* **260**, 176 (1993).
15. The authors acknowledge funding from the National Science and Engineering Research Council of Canada's Operating grant program.

9 February 1994; accepted 30 March 1994

Simulating the Adsorption of Alkanes in Zeolites

Berend Smit* and J. Ilja Siepmann†

The configurational-bias Monte Carlo technique is applied to simulate the adsorption of long chain alkanes in zeolites. This simulation technique is several orders of magnitude more efficient than conventional methods that can be used to simulate the adsorption of long chain alkanes. The calculated heats of adsorption are found to be in excellent agreement with experimental data. The results show a surprising chain length dependence of the heats of adsorption. This dependence has a simple molecular explanation in terms of preferential siting of the long chain alkanes.

Zeolites are crystalline inorganic polymers that form a three-dimensional network of micropores. These pores are accessible to various guest molecules. The large internal surface, the thermal stability, and the presence of acid sites make zeolites an important class of catalytic materials for petrochemical applications. For a rational use of zeolites, it is essential to have a detailed knowledge of the behavior of the adsorbed molecules inside the pores of the zeolites. Unfortunately, such information is very difficult to obtain, particularly for long chain hydrocarbon molecules.

Catalytic conversion inside the pores of a zeolite can be seen schematically as a three-step process: (i) the adsorption and diffusion of the reactants, (ii) the catalytic conversion, and (iii) the diffusion and desorption of products from the zeolite. The overall activity and selectivity of a particular reaction is the result of a delicate balance of these three processes. Much experimental and theoretical effort is directed toward obtaining a detailed understanding of each of these steps at a molecular level (*1*). The high selectivity of zeolites implies that the behavior of the adsorbed molecules is system-specific. It is therefore essential to be able to study the behavior of the adsorbed molecules of interest under reaction conditions.

B. Smit, Shell Research B.V. Koninklijke/Shell-Laboratorium, Amsterdam, Post Office Box 38000, 1030 BN Amsterdam, Netherlands.
J. I. Siepmann, Department of Chemistry, University of Pennsylvania, Philadelphia, PA 19104–6323, USA.

*To whom correspondence should be addressed.
†Permanent address: Department of Chemistry, University of Minnesota, 207 Pleasant Street SE, Minneapolis, MN 55455, USA.

Computer simulations, used with molecular dynamics or Monte Carlo techniques, are an attractive alternative to experiments because these methods can, in principle, provide information for conditions under which experiments are not feasible. Indeed, over the last few years there has been considerable progress in simulating adsorption in zeolites [for a recent review, see (*2*)]. In practice, however, computer simulations have been limited to atoms or small molecular guest molecules and could not be extended to molecules of catalytic relevance. These limitations are discussed by June *et al.* (*3*); in this work, molecular dynamics was used to study the behavior of butane and hexane in the zeolite silicalite. June *et al.* observed that the diffusion of these alkanes is very slow and the rate of diffusion decreases with increasing chain length. Therefore, long simulations are required to obtain reliable results.

The Monte Carlo technique is not limited by the slow diffusion of the molecules, because moves can be made to arbitrary positions in the zeolite. For chain molecules, however, this is not the case because the probability of finding a position without overlap between hydrocarbon and zeolite decreases exponentially with chain length. Recently, we have developed a method, configurational-bias Monte Carlo, to simulate chain molecules (*4*, *5*). We demonstrate here that this approach can be used to study the behavior of long chain hydrocarbons in zeolites and allows us to address the much debated question of the preferential adsorption of the *n*-alkanes in the different channels of silicalite.

We used the configurational-bias Monte Carlo technique to study the adsorption of *n*-butane to *n*-dodecane in silicalite. In contrast to the conventional Monte Carlo technique, in the configurational-bias Monte Carlo technique a molecule is not inserted at random but is grown atom by atom such that overlap with the zeolite atoms is avoided (Fig. 1). This growing process introduces a bias that is removed by adjusting the acceptance rules (*4*–*7*). A simulation is performed in cycles, and each cycle consists of a number of randomly selected moves: displacement of particles, rotation of particles, partial regrowing of a molecule, and regrowing of a molecule at a randomly selected position. For the latter two moves, the configurational-bias Monte Carlo technique is used with a total simulation consisting of at least 10^6 cycles. The alkanes are described with the model of (*8*). This model yields an accurate description of their phase behavior. Following Kiselev and co-workers (*9*), we assume that the zeolite lattice is rigid and that the zeolite-alkane interactions are dominated by dispersive interactions. Lattice vibrations can have a pronounced effect on the diffusion because these vibrations may lower the diffusional barriers. Because these barriers hardly contribute to the equilibrium distribution, we expect that the effect of lattice vibrations on the equilibrium properties is small. The details of the model are given in Table 1.

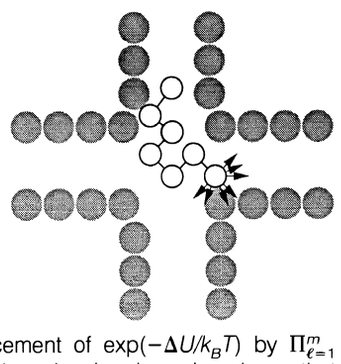

Fig. 1. Schematic drawing of the growing of an alkane in a zeolite in a configurational-bias Monte Carlo move. The black circles represent the atoms of the zeolite, and the white circles represent the atoms of the alkane. Seven atoms have been grown successfully, and an attempt is made to insert the eighth. The arrows indicate seven trial positions for which the energy u_i is calculated. Out of these seven positions one is selected with a probability $p_i = \exp(-u_i/k_BT)/w_{new}(\ell)$ with $w_{new}(\ell) = \Sigma_j \exp(-u_j/k_BT)$, where T is the temperature and k_B is Boltzmann's constant. Similarly, for the old configuration we calculate $w_{old}(\ell) = \Sigma_j \exp(-u_j/k_BT)$. This is repeated until the entire chain of length m has been grown. It can be proven (*5*) that the bias of the growing is removed by the replacement of $\exp(-\Delta U/k_BT)$ by $\Pi_{\ell=1}^{m} w_{new}(\ell)/\Pi_{\ell=1}^{m} w_{old}(\ell)$ in the acceptance rule. Comparison with molecular dynamics shows that configurational-bias Monte Carlo is two orders of magnitude more efficient for butane and up to 12 orders of magnitude more efficient for dodecane.